J Mater Sci (2008) 43:43–54
DOI 10.1007/s10853-007-2126-4

Effect of mechanical properties on wrinkling limit diagrams for Aluminum 5086 alloy annealed at different temperature

R. Narayanasamy · J. Satheesh · C. Loganathan

Received: 10 April 2007 / Accepted: 22 August 2007 / Published online: 27 September 2007
© Springer Science+Business Media, LLC 2007

Abstract This article deals with the wrinkling limit diagrams for Aluminium 5086 alloy sheets having thickness of 2.00 mm annealed at three different temperatures namely 200, 250 and 300 °C. The study pertains to deep drawing into cylindrical cups through conical die using a flat bottom punch. When a conical die is employed, the need for a hold down or clamping ring is eliminated. However, this enhances the propensity of the blank to fail by wrinkling or buckling, particularly in the early stages of a drawing process in which thin sheet blanks are used. It is proved by these researchers and others that the onset of wrinkling takes place when the ratio of strain increments ($d\varepsilon_r/d\varepsilon_\theta$) or the ratio of strain ($\varepsilon_r/\varepsilon_\theta$) reaches a critical value during the drawing process. These values which could be determined experimentally over which the wrinkling takes place has been shown in the form of wrinkling limit diagrams for the above grade at different annealed temperatures. An attempt is also made to develop the wrinkling theory that predicts the wrinkling based on results obtained in the form of wrinkling limit diagrams established for the above grade at different annealed temperatures. Further it was observed that the annealed sheets having high *n*-value, high *R*-value and high UTS/σ_y ratio improve the resistance against wrinkling.

R. Narayanasamy (✉) · J. Satheesh
Department of Production Engineering, National Institute of Technology, Tiruchirappalli 620015 Tamil Nadu, India
e-mail: narayan@nitt.edu

J. Satheesh
e-mail: satheesh_ait@yahoo.com

C. Loganathan
Department of Mechanical Engineering, Saranathan College of Engineering, Venkateshwara Nagar, Tiruchirappalli 620012 Tamil Nadu, India
e-mail: bkloganathanc@yahoo.co.in

Nomenclature

n_{av}	Average strain hardening index value.
n_{av}	0.25 (n_0 + 2n_{45} + n_{90})
k_{av}	Average strength coefficient
k_{av}	0.25 (k_0 + 2k_{45} + k_{90})
R	Average normal anisotropy
R	0.25(R_0 + 2R_{45} + R_{90})
x_{av}	0.25 (x_0 + 2x_{45} + x_{90})
σ_y (average)	$0.25\ (\sigma_{y_0} + 2\sigma_{y_{45}} + \sigma_{y_{90}})$
σ_u (average)	$0.25\ (\sigma_{u_0} + 2\sigma_{u_{45}} + \sigma_{u_{90}})$
σ_r	Radial stress
σ_θ	Hoop stress
$\bar{\sigma}$	Effective stress
ε_r	Radial strain
ε_θ	Hoop strain
$\bar{\varepsilon}$	Effective strain
$d\sigma_r$	Radial stress increment
$d\sigma_\theta$	Hoop stress increment
$d\varepsilon_r$	Radial strain increment
$d\varepsilon_\theta$	Hoop strain increment
$d\bar{\varepsilon}$	Effective strain increment
$d\gamma_{max}$	Maximum shear strain increment
γ_{max}	Maximum shear strain
τ_{max}	Maximum shear stress
α	Ratio of in-plane stress increments
β	Ratio of in-plane strain increments
a	Yielding behaviour constant

Introduction

Influence of annealing of commercially pure (CP) Aluminium was evaluated by aspects namely microstructure, mechanical properties, electrical conductivity, and general corrosion. It is shown that by selecting optimal annealing

condition result in ultra fine grains in CP Aluminium with good combination of high strength and ductility as explained elsewhere [1]. Using an Al-Mg-Cu alloy developed for auto body panels, strip sheets are experimentally produced by various cold-rolling and annealing procedures. Tensile and metallographic properties of the sheets and their relations are examined to attain high formability. The elongation is closely related to the grain size, and increases with the final annealing temperature as described by Takuda et al. [2]. The suitability of recently developed aluminium alloys (an Al–Mg–Mn alloy and an Al–Li–Cu alloy) for press-forming applications has been examined. The characterization involved the experimental determination of microstructural aspects, tensile properties and formability parameters such as average plastic strain ratio and planar anisotropy. These alloys are suitable for stamping applications where stretching constitutes the major proportion of the deformation [3, 4]. In the sheet metal forming, production engineers and researchers have paid much attention to the behaviour of wrinkling in sheet metal forming operations over the last decade. It is difficult to define criteria for describing the stability in metal forming. In general, wrinkling may be affected by various factors including material properties, punch and die geometry, blank geometry, holding conditions, interface friction and lubrication state. Numerous studies have been carried out on the relationship between wrinkling and material characteristics [5–14]. One of the most representative work was performed by Yoshida [10] and was generally directed towards investigation of the conditions under which wrinkling would occur in a large shallow pressing, characterized by the well-known Yoshida buckling test. Karima and Sowerby [15] have attempted a bifurcation approach to the study of wrinkling during deep drawing. They treated flange wrinkling during deep drawing without a blank holder as a problem of elastic-plastic buckling of an annular plate. Their results indicate that a high rate of hardening has a favourable effect on the prevention of buckling when deep drawing through Conical and tapered dies. However, Narayanasamy and Sowerby [16] have showed that the stainless steel 304 sheets which have a low value of normal anisotropy and a high value of normalized hardening rate, have better resistance to the formation of wrinkles. The wrinkling behaviour of cold-rolled sheet metals with the aim of prediction of the onset of wrinkling during drawing through Tractrix and Conical dies, has been studied in addition [8]. Di and Thomson [17] have used the neural network principle for the prediction of strain at the onset of wrinkling, based on the Yoshida material parameters. The effect of geometrical variables that affect the onset of wrinkling during deep drawing has been investigated by Wang et al. [18], using a neural network approach.

Kim and Son [19] studied wrinkling behaviour of sheet metals using a numerical analysis for evaluating a wrinkling limit diagram (WLD) for an anisotropic sheet subjected to biaxial plane stress. The scheme of plastic bifurcation theory for thin shells based on the Donnell-Mushtari-Vlasov shell theory is used. The effects of various material parameters namely yield stress, strain hardening coefficient and normal anisotropy and geometrical parameters on the wrinkling limit diagram were investigated numerically and compared with the results of the experiments of Kawai and Havrnek. The formation of wrinkles can be predicted by analytical treatments using Hill's [20] bifurcation criterion, specialized by Hutchinson [21] to the case of thin and shallow plates and shells.

In the present work, an attempt is made to predict the onset of wrinkling using wrinkling limit diagram for Aluminium 5086 alloy at different annealed temperatures.

Experimental work

Cold-rolled Aluminium 5086 alloy sheet metal having thickness 2.00 mm were subjected to three different annealing treatments namely (1) heating temperature 200 °C, soaking (maintaining constant temperature in the furnace) time 1 h and furnace cooling (HT1), (2) heating temperature 250 °C, soaking time 1 h and furnace cooling (HT2) and (3) heating temperature 300 °C, soaking time 1 h and furnace cooling (HT3). An ordinary muffle furnace was used for heating the aluminium alloy sheets. Aluminium 5086 alloy grade with different mechanical properties were selected for this work, as shown in Tables 2–4. Table 1 shows the chemical composition of the above said sheet metals. These sheet metals were purchased from the Indian market in cold-rolled condition. Since the sheet metals are anisotropy in nature, the normal anisotropy parameter (R) was evaluated as shown in Refs. [19, 20]. This is defined as

$$R = 0.25(R_0 + 2R_{45} + R_{90}) \quad (1)$$

where 0, 45 and 90 represents rolling direction, 45° to rolling direction and transverse direction respectively. R is the plastic strain ratio. Tables 2–4, present some typical results of the R-values obtained for the annealed Aluminium 5086 alloy grade with three different heat-treated conditions. Using the tensile test, all mechanical properties

Table 1 Chemical composition of Aluminium 5086 Alloy (in wt.%)

Material	Mg	Mn	Si	Fe	Cr	Cu	Ti	Zn
Al 5086 alloy	4.0	0.5	0.3	0.5	0.25	0.10	0.15	0.25

Table 2 Tensile properties of Aluminium 5086 alloy annealed at 200 °C

Orientation relative to rolling direction	Strain hardening exponent n	Strength coefficient K (MPa)	R	Yield stress σ_y (MPa)	Ultimate tensile stress (Mpa)	UTS/σ_y	%Elongation
0°	0.178	410	0.790	245 Average	323 Average	1.323	10.36
45°	0.098	440					
90°	0.189	450					
Average*	0.1407	435					

* Average = $(x_0 + 2x_{45} + x_{90})/4$, where x is n-value or K-value

Table 3 Tensile properties of Aluminium 5086 alloy annealed at 250 °C

Orientation relative to rolling direction	Strain hardening exponent n	Strength coefficient K (MPa)	R	Yield stress σ_y (MPa)	Ultimate tensile stress (Mpa)	UTS/σ_y	%Elongation
0°	0.176	410	1.013	222 Average	315 Average	1.42	11.62
45°	0.188	490					
90°	0.172	450					
Average*	0.181	460					

* Average = $(x_0 + 2x_{45} + x_{90})/4$, where x is n-value or K-value

Table 4 Tensile properties of Aluminium 5086 alloy annealed at 300 °C

Orientation relative to rolling direction	Strain hardening exponent n	Strength coefficient K (MPa)	R	Yield stress σ_y (MPa)	Ultimate tensile stress (Mpa)	UTS/σ_y	%Elongation
0°	0.259	480	1.128	210 Average	303 Average	1.44	13.64
45°	0.261	550					
90°	0.142	460					
Average*	0.231	510					

* Average = $(x_0 + 2x_{45} + x_{90})/4$, where x is n-value or K-value

were determined for the above grade of sheet metals and the same is shown in Tables 2–4.

The drawing experiments were also conducted as per schedule described elsewhere [16], using conical die for the three different heat-treated Aluminium 5086 alloy grade. The blanks having different diameters were drawn through the die with no lubricant. A grid consisting of circles of 3.5 mm in diameter was printed on the blanks for the determination of the strain distribution. The grid circles were printed on blanks by using electrochemical etching process. The grid measurements reveal the onset of wrinkling in the stage of bending or tube sinking. The blanks were partially drawn through the die to about 10 or more different depths until the wrinkling developed and the grid circles measured on each of the partially drawn sheets in a region close to the rim of the blank where wrinkling generally developed. The strains, namely, hoop (ε_θ) and radial (ε_r) were calculated from the grid measurement data. The modes of the wrinkling developed during drawing tests were explained in Refs. [22, 23]. **Figure 1a–c show the sample distribution of the radial and hoop strains for different Aluminium alloy blanks of grade Aluminium 5086 alloy which is subjected to three different types of heat treatments as said above. From these figures it is noted that the slope of the ε_r–ε_θ strain curve changes suddenly when a wrinkle develops on the blank. The reason for this is that there is an increase in circumferential strain (ε_θ) when the wrinkle is about to develop on the blank.

Theoritical analysis

Theory of plasticity

The wall section of a truncated Conical cup (a partially drawn cup) is approximated to a flat strip of width 'a_1' and height 'b_1' as shown in the Fig. 2a, corresponding respectively to the mean circumference and the generator of the cone. The strip is subjected to plane stress, specified by σ_r and σ_θ .

Assuming the material to be rigid-plastic and obeying the Hill new yield criterion [20] together with the

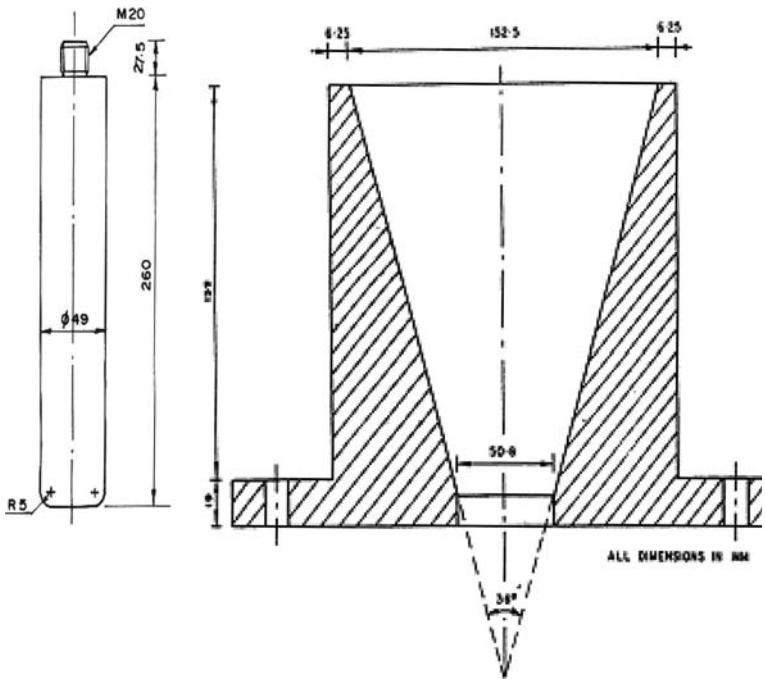

Fig. 1 Conical die and flat bottomed punch

Levy-Mises flow rule, the increments of strain can be expressed as follows:

$$\begin{aligned} d\varepsilon_1 &= d\lambda[(\sigma_1+\sigma_2)^{a-1} + (1+2R)(\sigma_1-\sigma_2)^{a-1}] \\ d\varepsilon_2 &= d\lambda[(\sigma_1+\sigma_2)^{a-1} - (1+2R)(\sigma_1-\sigma_2)^{a-1}] \\ d\varepsilon_3 &= -d\lambda[2(\sigma_1+\sigma_2)^{a-1}] \end{aligned} \tag{2}$$

where 'a' is yielding behaviour constant.

The ratio of the in-plane strain increments can be expressed as

$$\frac{d\varepsilon_2}{d\varepsilon_1} = \frac{(\sigma_1+\sigma_2)^{a-1} - (1+2R)(\sigma_1-\sigma_2)^{a-1}}{(\sigma_1+\sigma_2)^{a-1} + (1+2R)(\sigma_1-\sigma_2)^{a-1}} \tag{3}$$

Expression 3 can be rewritten as

$$\beta = \frac{(1+\alpha)^{a-1} - (1+2R)(1-\alpha)^{a-1}}{(1+\alpha)^{a-1} + (1+2R)(1-\alpha)^{a-1}} \tag{4}$$

where

$$\alpha = \frac{\sigma_2}{\sigma_1} = \frac{\sigma_\theta}{\sigma_r} \qquad \text{and} \qquad \beta = \frac{d\varepsilon_2}{d\varepsilon_1} = \frac{d\varepsilon_\theta}{d\varepsilon_r} \tag{5}$$

The constant 'a' provided in the Eqs. 2–4 represents the yielding behaviour of metals.

The quantities α and β are the ratios of the in-plane stress and the in-plane plastic strain increments, respectively. Hence, if the ratio of the stress is known, the ratio of the strain increments can be determined and *vice versa*. For wrinkling to occur, it is necessary that σ_θ should be compressive (i.e. α should be negative).

As per Hill's old yield criterion [20], putting $a = 2$, expression 4 becomes

$$\beta = \frac{(1+\alpha) - (1+2R)(1-\alpha)}{(1+\alpha) + (1+2R)(1-\alpha)} \tag{6}$$

In expression 6 α takes the value of zero to infinity. Substituting the limiting values

$$\beta = \frac{-R}{(1+R)} \qquad (\text{when } \alpha = 0)$$

and (7)

$$\beta = \frac{-(1+R)}{R} \qquad (\text{when } \alpha = \infty)$$

when R takes the value of unity:

$$-2 < \beta < -1/2 \tag{8}$$

This relationship is true irrespective of whether the material work-hardens or not. The above relationship (refer Eq. 7) is independent of the yielding behaviour constant 'a'. This can be checked without substituting the value of 2.0 for the above constant 'a', in the Eq. 4, provided in the above. As shown in Fig. 2b, this situation can be represented in principal stress space and principal strain space. The Eq. 6 can be rearranged as follows:

$$\alpha = \frac{R(1+\beta)+\beta}{R(1+\beta)+1} \tag{9}$$

Using the Eq. 9, for the known values of β and R, the value of α can be determined.

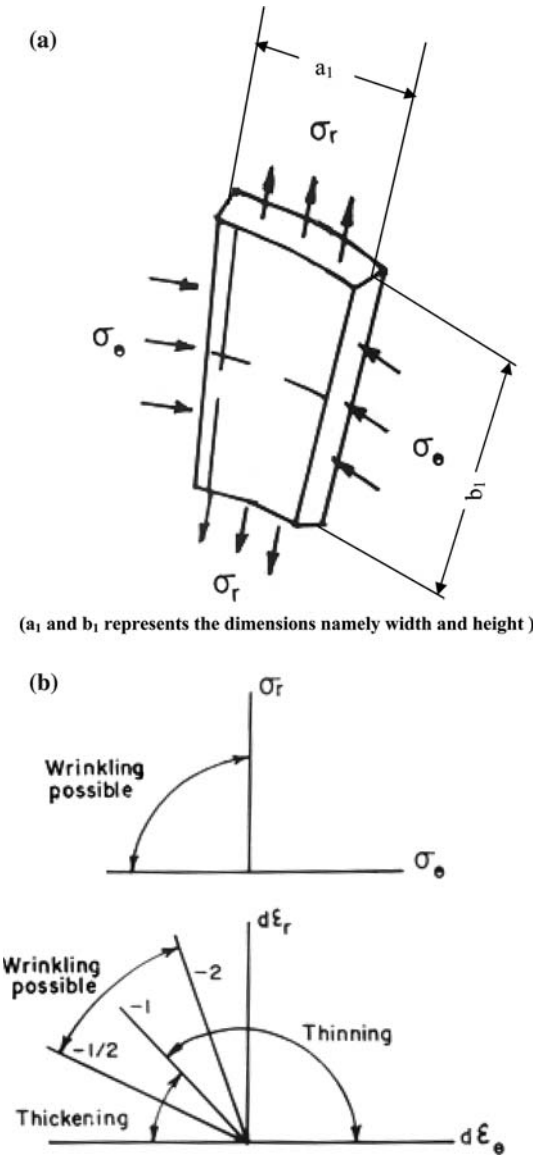

Fig. 2 (**a**) Stress state in the cup wall, (**b**) Wrinkling tendencies shown in stress and strain space [5]

As described elsewhere [24], the effective strain increment can be written as follows:

$$d\bar{\varepsilon}=\sqrt{2/3}\left[\frac{(2+R)(1+R)}{(1+2R)}\left\{d\varepsilon_r^2+d\varepsilon_\theta^2+\left(\frac{2R}{1+R}\right)d\varepsilon_r d\varepsilon_\theta\right\}\right]^{0.5} \tag{10}$$

The Eq. 10 can also be written as follows:

$$\frac{d\bar{\varepsilon}}{d\varepsilon_r}=\sqrt{2/3}\left[\frac{(2+R)(1+R)}{(1+2R)}\left\{1+\left(\frac{d\varepsilon_\theta}{d\varepsilon_r}\right)^2+\left(\frac{2R}{1+R}\right)\frac{d\varepsilon_\theta}{d\varepsilon_r}\right\}\right]^{0.5} \tag{11a}$$

Similarly,

$$\frac{d\bar{\varepsilon}}{d\varepsilon_\theta}=\sqrt{2/3}\left[\frac{(2+R)(1+R)}{(1+2R)}\left\{1+\left(\frac{d\varepsilon_r}{d\varepsilon_\theta}\right)^2+\left(\frac{2R}{1+R}\right)\frac{d\varepsilon_r}{d\varepsilon_\theta}\right\}\right]^{0.5} \tag{11b}$$

For the known values of $d\varepsilon_r$ and $d\varepsilon_\theta$, the effective strain increment $d\bar{\varepsilon}$, the ratio $(d\bar{\varepsilon}/d\varepsilon_r)$ and the ratio $(d\bar{\varepsilon}/d\varepsilon_\theta)$ can be determined.

As described elsewhere [24], the yield function can be described as follows:

$$\sigma_r^2+\sigma_\theta^2-\left(\frac{2R}{1+R}\right)\sigma_r\sigma_\theta=\bar{\sigma}^2 \tag{12}$$

The Eq. 11 can be described as follows:

$$\left(\frac{\sigma_r}{\bar{\sigma}}\right)^2=\left(1+\alpha_1^2-\frac{2R\alpha_1}{(1+R)}\right)^{-1} \tag{13a}$$

and

$$\left(\frac{\sigma_\theta}{\bar{\sigma}}\right)^2=\left(1+\alpha_2^2-\frac{2R\alpha_2}{(1+R)}\right)^{-1} \tag{13b}$$

where, σ_r is the radial stress, σ_θ is the hoop stress, $\bar{\sigma}$ is the effective stress, R is the normal anisotropy, $\alpha_1=\sigma_\theta/\sigma_r$ and $\alpha_2=\sigma_r/\sigma_\theta$.

From Eq. 13a and b for known values of α_1, α_2 and R, the stress ratios $(\sigma_r/\bar{\sigma})$ and $(\sigma_\theta/\bar{\sigma})$ can be determined.

For sheet metals used in industries, the value of R (the normal anisotropy) varies from 0.25 to 3.00. Therefore, the limiting strain increments ratio (β) can be determined using Eq. 7 and the same is reported in Table 3. Table 3 shows that the strain increments ratio value depends upon R-value only. However, it is already proved by Narayanasamy and Sowerby [16] that the strain increments ratio value also depends upon the strain hardening exponent value apart from R-value for the case of austenitic stainless steels (grades 301, 302 and 304) due to the formation of plastically strain induced martensite.

According to Mohr's circle drawn between $d\varepsilon_r$ (the radial strain increments) and $d\varepsilon_\theta$ (the hoop strain increment), the following expression can be written.

$$d\gamma_{max}=\frac{1}{2}(d\varepsilon_r+d\varepsilon_\theta) \tag{14}$$

where $d\gamma_{max}$ represents the maximum shear strain increment value, which is nothing but the radius of Mohr's circle.

The Eq. 14 can be written as follows:

$$\frac{d\gamma_{max}}{d\varepsilon_\theta} = \frac{1}{2}\left[\frac{d\varepsilon_r}{d\varepsilon_\theta} + 1\right]$$
$$\frac{d\gamma_{max}}{d\varepsilon_r} = \frac{1}{2}\left[\frac{d\varepsilon_\theta}{d\varepsilon_r} + 1\right] \quad (15)$$

Since the value of $(d\varepsilon_r/d\varepsilon_\theta)$ is known, the values of $(d\gamma_{max}/d\varepsilon_\theta)$ and $(d\gamma_{max}/d\varepsilon_r)$ can be determined using Eq. 15. If we assume that the strain proportional, then

$$\frac{d\varepsilon_\theta}{d\varepsilon_r} = \frac{\varepsilon_\theta}{\varepsilon_r} \quad (16)$$

Therefore, the Eq. 15 can be modified as follows

$$\frac{\gamma_{max}}{\varepsilon_\theta} = \frac{1}{2}\left[\frac{\varepsilon_r}{\varepsilon_\theta} + 1\right]$$
$$\frac{\gamma_{max}}{\varepsilon_r} = \frac{1}{2}\left[\frac{\varepsilon_\theta}{\varepsilon_r} + 1\right] \quad (17)$$

Since the deformation is under plane stress, only stresses namely σ_r and σ_θ are present. Therefore, the following expressions can be written with similar to Eqs. 15 and 17.

$$\frac{\tau_{max}}{\sigma_\theta} = \frac{1}{2}\left[\frac{\sigma_r}{\sigma_\theta} + 1\right]$$
$$\frac{\tau_{max}}{\sigma_r} = \frac{1}{2}\left[\frac{\sigma_\theta}{\sigma_r} + 1\right] \quad (18)$$

Here, τ_{max} is the maximum shear stress developed, which is nothing but the radius of the Mohr's circle.

The Eq. 10 can be written as follows for the determination of the effective strain providing the strain is proportional.

$$\bar{\varepsilon} = \sqrt{2/3}\left[\frac{(2+R)(1+R)}{1+2R}\left\{\varepsilon_r^2 + \varepsilon_\theta^2 + \left(\frac{2R}{1+R}\right)\varepsilon_r\,\varepsilon_\theta\right\}\right]^{0.5} \quad (19)$$

The Eq. 19 can be rearranged as follows:

$$\frac{\bar{\varepsilon}}{\varepsilon_r} = \sqrt{2/3}\left[\frac{(2+R)(1+R)}{(1+2R)}\left\{1 + \left(\frac{\varepsilon_\theta}{\varepsilon_r}\right)^2 + \left(\frac{2R}{1+R}\right)\frac{\varepsilon_\theta}{\varepsilon_r}\right\}\right]^{0.5} \quad (20a)$$

$$\frac{\bar{\varepsilon}}{\varepsilon_\theta} = \sqrt{2/3}\left[\frac{(2+R)(1+R)}{(1+2R)}\left\{1 + \left(\frac{\varepsilon_r}{\varepsilon_\theta}\right)^2 + \left(\frac{2R}{1+R}\right)\frac{\varepsilon_r}{\varepsilon_\theta}\right\}\right]^{0.5} \quad (20b)$$

For known values of ε_r and ε_θ, the effective strain $\bar{\varepsilon}$ and strain ratios namely $\left(\frac{\bar{\varepsilon}}{\varepsilon_r}\right)$ and $\left(\frac{\bar{\varepsilon}}{\varepsilon_\theta}\right)$ can be determined.

Results and discussion

Chemical composition and microstructure

The chemical composition for Al 5086 alloy tested is provided in Table 1, and the metallurgical microstructure of Aluminium 5086 alloy annealed at three different temperatures details are provided in Fig. 3.The microstructure

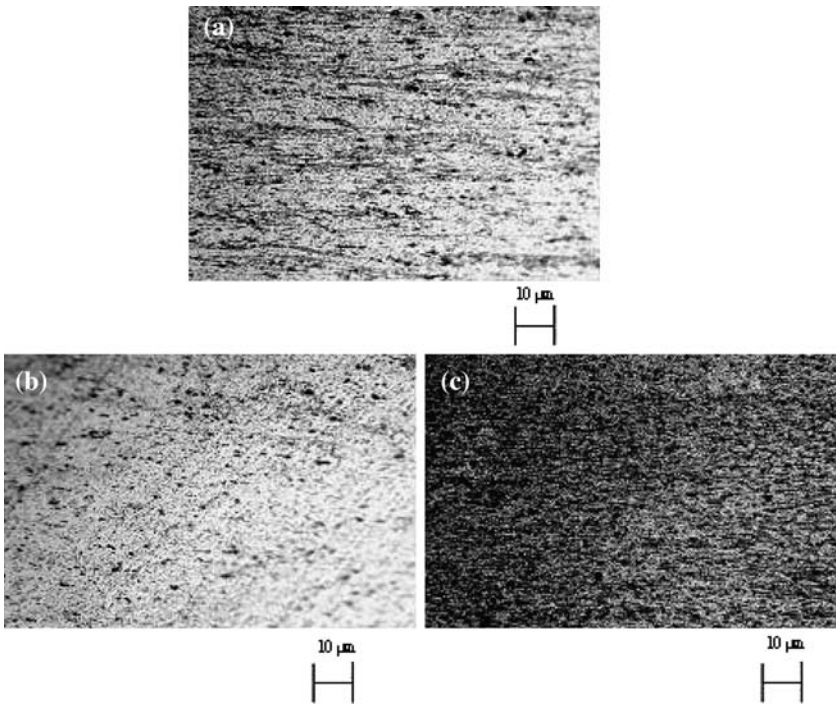

Fig. 3 (**a**) Microstructure of Al 5086 annealed at 200 °C at magnification 400×, (**b**) Microstructure of Al 5086 annealed at 250 °C at magnification 400×, (**c**) Microstructure of Al 5086 annealed at 300 °C at magnification 400×

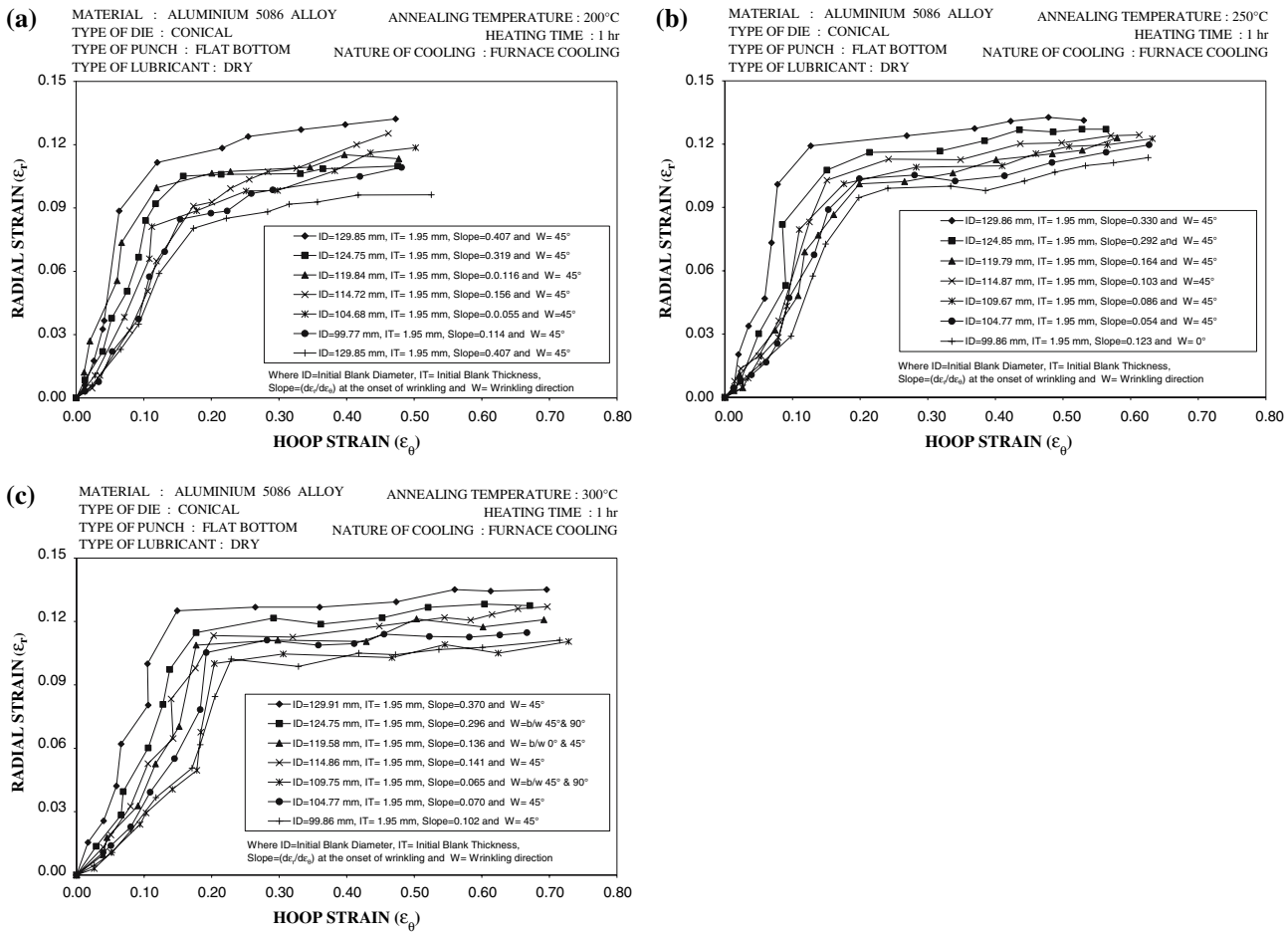

Fig. 4 (**a**–**c**) Variation of the radial strain with respect to the hoop strain

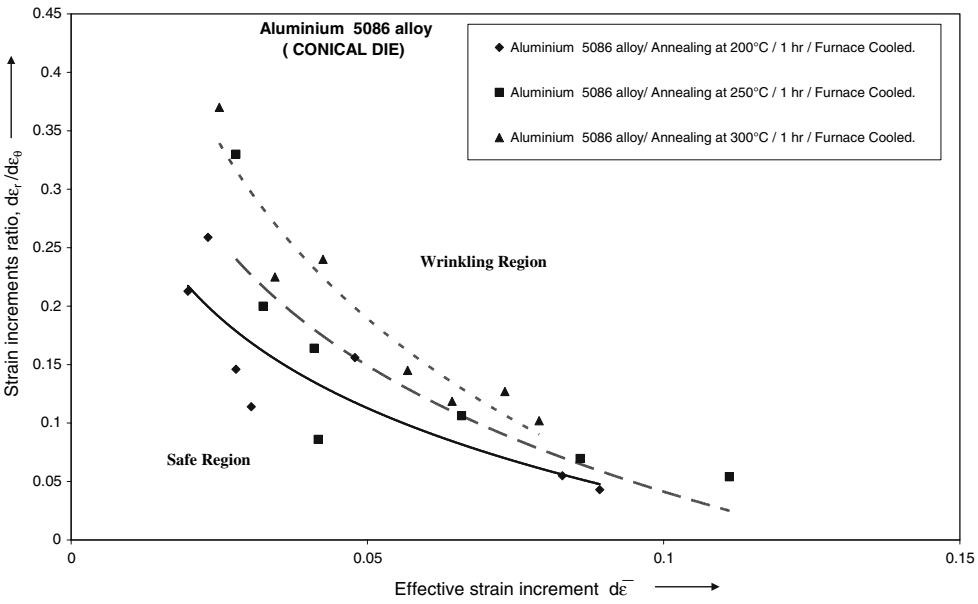

Fig. 5 Wrinkling limit diagram in terms of strain increments ratio for Aluminium 5086 alloy

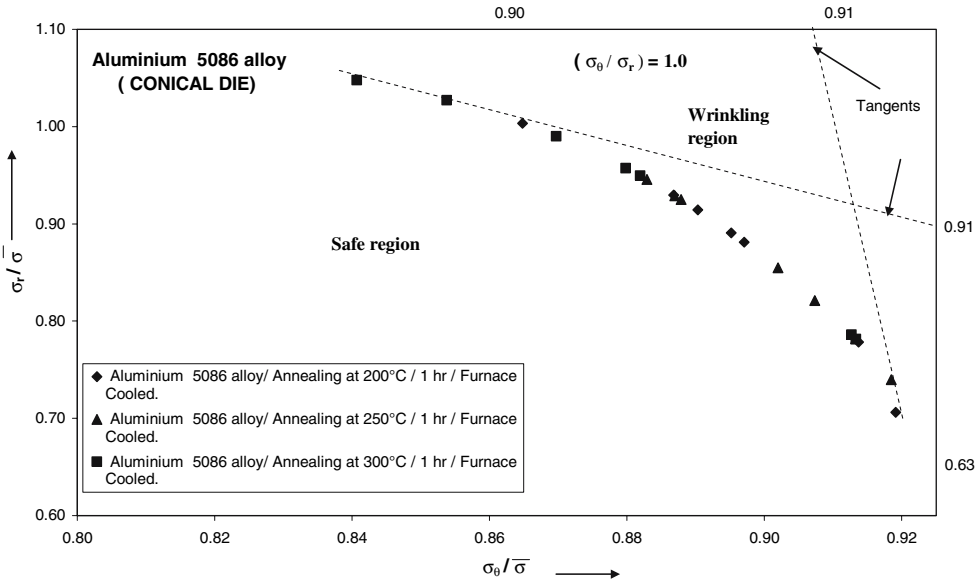

Fig. 6 Wrinkling limit diagram in terms of stress ratio for Aluminium 5086 alloy

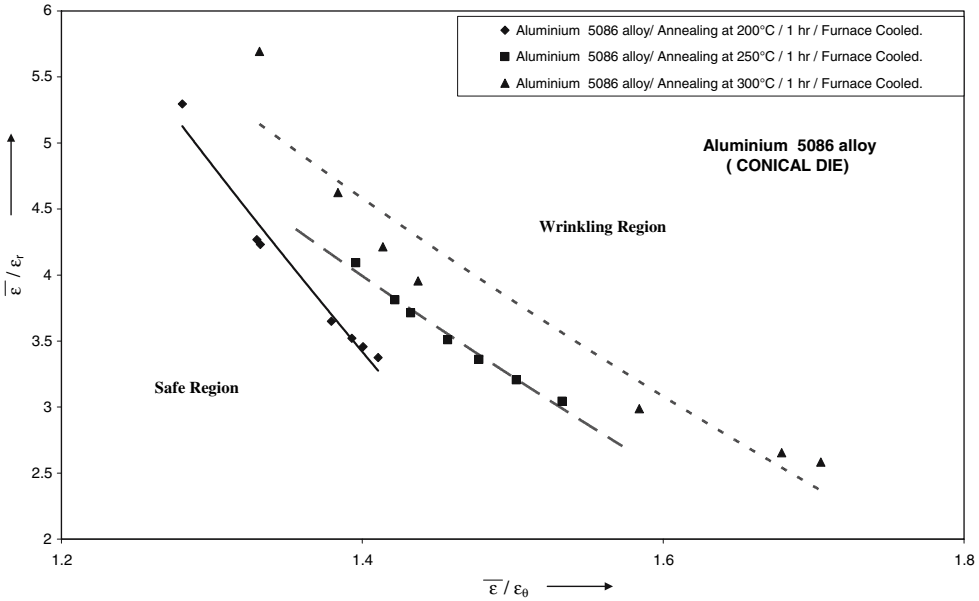

Fig. 7 Wrinkling limit diagram in terms of strain ratios for Aluminium 5086 alloy

of the sheet annealed at 200 °C shows partial recovery and no recrystallization. The microstructure of sheets annealed at 250 °C shows fully recovered and partial recrystallized grain structure whereas, sheets annealed at 300 °C show very fine partially recrystallized grains. A fundamental understanding that 5086 is a medium-to-high strength non-heat-treatable alloy. The alloy has good formability than alloy 5083. As this alloy is resistant to stress corrosion cracking and exfoliation, it has wide application in the marine industry [25, 26]. The magnesium in the Al 5086 is 4.0%, the presence of magnesium in larger quantity retards formability but enhances castability and strength. The percentage of iron in the material is 0.50%, its presence in the alloy increase the recrystallisation temperature. The presence of silicon is about 0.4% and it improves the fluidity of the alloy. The manganese and chromium jointly counteract the corrosion effect of Iron. Manganese and chromium have a strengthening effect with reduction of ductility. Copper content is about 0.10% and its presence, reduces pitting corrosion. The zinc that is present in 0.25% does not have effect on corrosion but enhances castability and strength. The solid solubility of magnesium in aluminium alloys ranges from 2% in room temperature and 14–15% at 720 K. Silicon usually forms Mg_2Si, mostly insoluble, especially the alloys with more than 3–4% magnesium. Iron may form $FeAl_3$ in the absence of chromium or manganese.

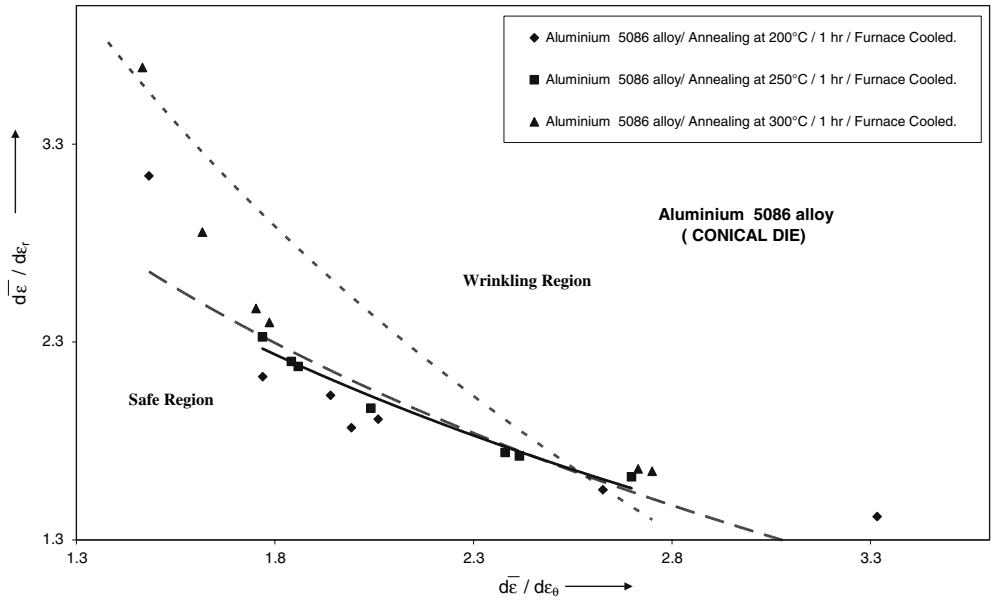

Fig. 8 Wrinkling limit diagram in terms of strain increments ratio for Aluminium 5086 alloy

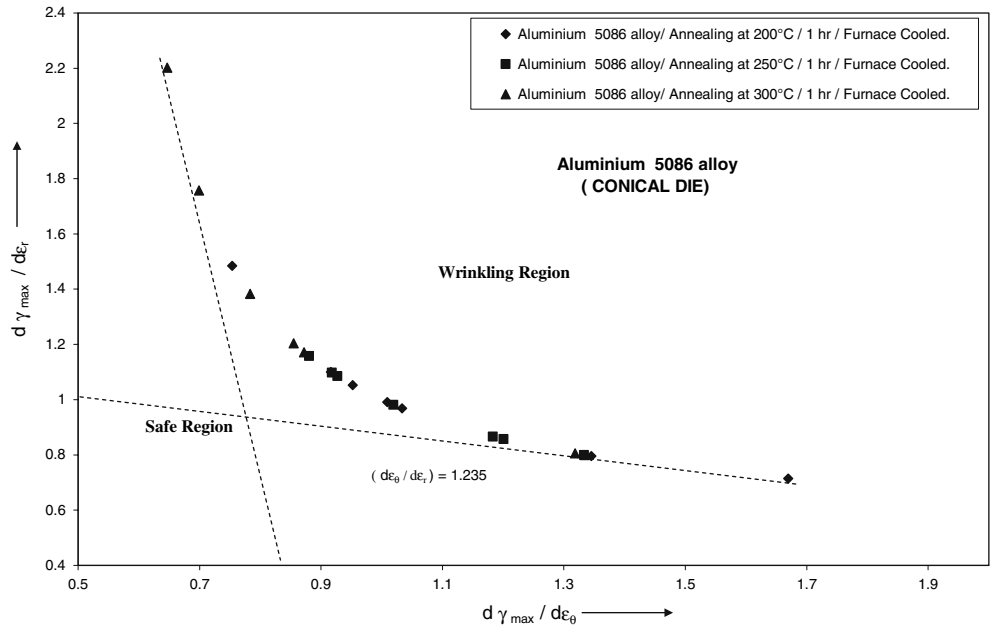

Fig. 9 Wrinkling limit diagram in terms of strain increments ratio for Aluminium 5086 alloy

Titanium remains mostly in solution. Titanium increases the recrystallisation temperature and aids in grain refinement.

Tensile properties

Tensile properties of sheets annealed at three different temperatures are shown in Tables 2–4. The average strain hardening exponent ($\bar{n}$) value indicates stretchability and formability [27, 28]. As the $\bar{n}$-value increases, the stretchability also increases. The sheet annealed at 200 °C, possess comparatively less average strength coefficient value (K) due to presence of cold-worked microstructure. Whereas, the grains in microstructure of the sheets annealed at 300 °C is partially recrystallized in nature and they possess higher K-value, the strength coefficient. The sheets annealed at 300 °C temperature possess a higher value of UTS, compared to other lower annealing temperatures but it possesses a low yield stress, compared to the rest. The percentage of elongation for sheets annealed at 300 °C is found to be 13.64, which

Table 5 Values of strain increments ratio (β) for various R-values

R-value	β-value when	
	$\alpha = 0.0$	$\alpha = \infty$
0.00	0.000	Infinity
0.25	0.200	5.000
0.50	0.333	3.000
0.75	0.4285	2.334
1.00	0.500	2.000
1.50	0.600	1.667
2.00	0.666	1.500
2.50	0.7142	1.400
3.00	0.750	1.333

Note: This table is derived using Eq. 7 explained in the text. Normal anisotropy (R) takes values from 0.25 to 0.30 for industrial sheet metals

is found to be greater than the sheet annealed at other two temperatures.

Wrinkling limit diagram

The ratio of strain increments ($d\varepsilon_r/d\varepsilon_\theta$) and the ratio of strains ($\varepsilon_r/\varepsilon_\theta$) at the onset of wrinkling can be obtained from the strain values namely ε_r and ε_θ measured for the drawing operation. The same is shown in the form of diagrams in Fig. 4a–c. Using the expressions provided by the theory of plasticity, the wrinkling limit diagrams in terms of strain increments ratio, strain ratio and stress ratio can be plotted as shown in this section.

Figure 5 has been plotted between the strain increments ratio ($d\varepsilon_r/d\varepsilon_\theta$) and the effective strain increment for the case of drawing of Aluminium 5086 alloy sheets annealed at 200, 250 and 300 °C through the conical die. It is observed that the strain increments ratio obtained at the onset of wrinkling is found to be a higher value for the Aluminium 5086 alloy sheet annealed at 300 °C comparing to other two annealed temperature 200 and 250 °C. Further, it is observed that the area of safe region is found to be greater for annealed temperature of 300 °C and lower for 200 °C. The behaviour of Aluminium 5086 alloy annealed at 250 °C is in between the sheets annealed at 200 and 300 °C.

Figure 6 has been plotted between the stress ratios, $(\sigma_r/\bar{\sigma})$, and $(\sigma_\theta/\bar{\sigma})$, for the onset of wrinkling when drawing through the conical die for the Aluminium 5086 alloy sheet annealed at three temperatures namely 200, 250 and 300 °C. It is observed that there is a clear curve, which separates the region from safe and the wrinkling region. The ratio of (σ_θ/σ_r) is found to be 1.0.

Figure 7 has been plotted between the strain ratios $(\bar{\varepsilon}/\varepsilon_r)$ and $(\bar{\varepsilon}/\varepsilon_\theta)$ obtained using Eq. 20, for Aluminium 5086 alloy sheet annealed at three different temperatures drawn through conical die. As said earlier, there is a clear demarcation curve between the safe region and the wrinkling region. This demonstrates that the Aluminium 5086 alloy sheet annealed at 300 °C accommodates more hoop strain and radial strains before the onset of wrinkling comparing to the other two temperatures. The safe region is found to be more for higher annealing temperature (300 °C).

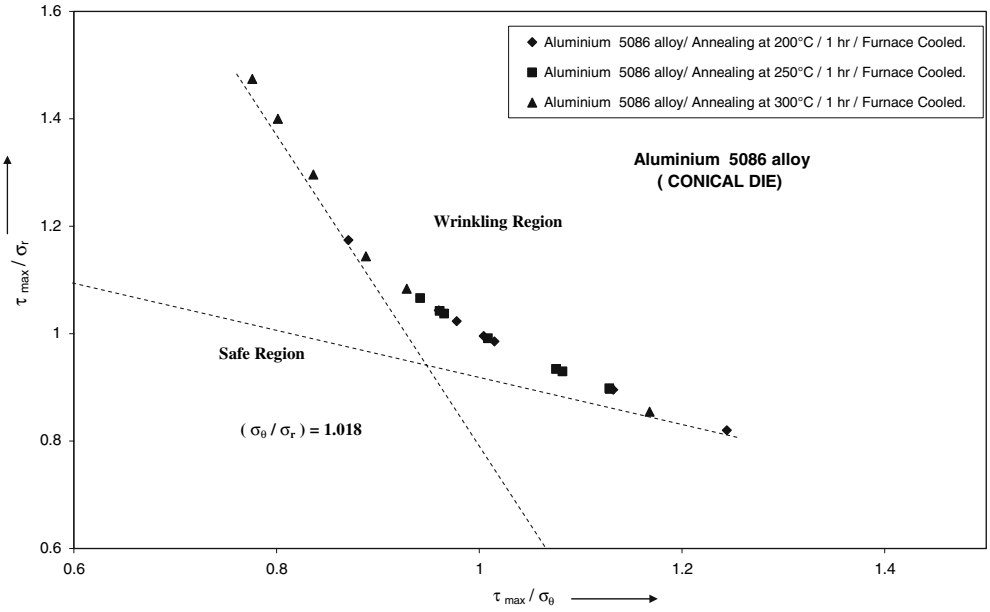

Fig. 10 Wrinkling limit diagram in terms of stress ratio for Aluminium 5086 alloy

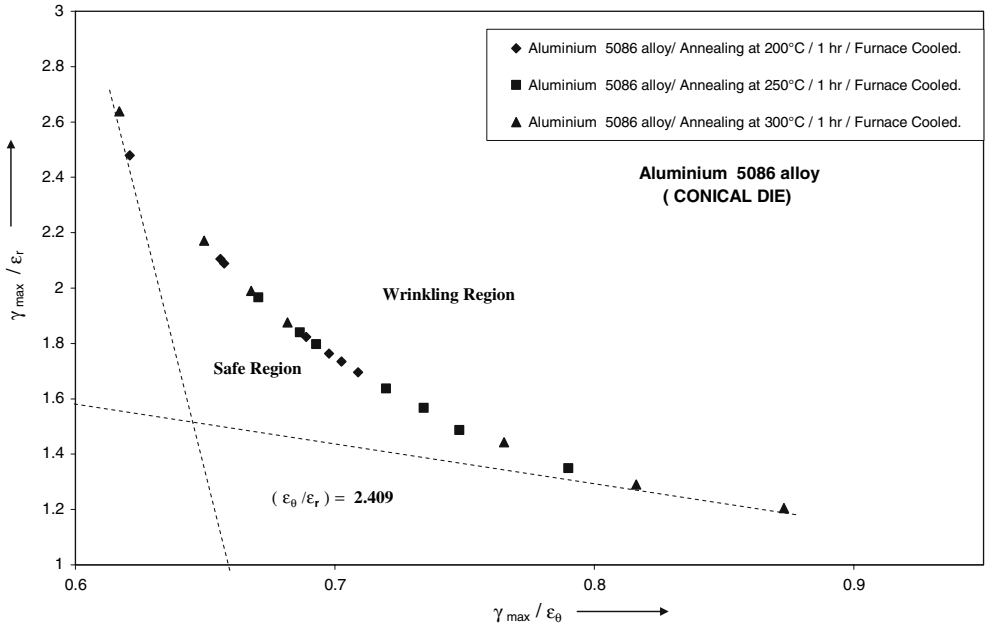

Fig. 11 Wrinkling limit diagram in terms of strain ratios for Aluminium 5086 alloy

Figure 8 has been plotted between the strain increment ratios $(d\bar{\varepsilon}/d\varepsilon_r)$ and $(d\bar{\varepsilon}/d\varepsilon_\theta)$ obtained using Eq. 11, for three different annealed temperatures for Aluminium 5086 alloy when drawn through conical die. For Aluminium 5086 alloy sheet annealed at 300 °C, the safe region is found to be the highest whereas for annealed at 200 °C the same region is found to be the lowest.

Figure 9 has been plotted between the strain increments ratios $(d\gamma_{max}/d\varepsilon_r)$ and $(d\gamma_{max}/d\varepsilon_\theta)$ for three different annealed temperatures for Aluminium 5086 alloy when drawn through conical die. It is observed that the strain increments ratio values obtained at the onset of wrinkling is found to fall in a single curve for three different annealed temperatures for Aluminium 5086 alloy. The wrinkling takes place over the strain increment $(d\gamma_{max}/d\varepsilon_\theta)$ range from 0.72 to 1.6 for the conical die and there is a clear demarcation curve between the safe region and the wrinkling region. As shown in Fig. 9, the limiting tangent values drawn from Y- and X-axis are 1.09 and 0.88, respectively and the ratio of β which is nothing but the ratio of $(d\varepsilon_\theta/d\varepsilon_r)$ is about 1.235. From Table 5, the theoretical value of ratio $(d\varepsilon_\theta/d\varepsilon_r)$ is also very close to 1.235 and therefore, both the theoretical and the experimental values of β matches each other, irrespective of the different annealed temperatures.

Figure 10 has been plotted between the stress ratio, (τ_{max}/σ_r) and ratio, $(\tau_{max}/\sigma_\theta)$, obtained using Eq. 18, for three different annealed temperatures for Aluminium 5086 alloy when drawn through conical die. It is noted that there is a clear demarcation line or curve between the safe region and the wrinkling region. As shown in this figure, the limiting tangent values drawn from Y- and X-axis are 1.10 and 1.06, respectively and the ratio of, α, which is nothing but the ratio of (σ_θ/σ_r) is about 1.0187 for conical die.

Figure 11 has been plotted between the strain ratios $(\gamma_{max}/\varepsilon_r)$ and $(\gamma_{max}/\varepsilon_\theta)$ obtained using Eq. 17, for three different annealed temperatures for Aluminium 5086 alloy when drawn through conical die. As mentioned earlier, there is a clear demarcation curve between the safe region and the wrinkling region for three different annealed temperatures. As shown in these figures, the limiting tangent values drawn from Y- and X-axis are 1.60 and 0.66, respectively and the ratio of $(\varepsilon_\theta/\varepsilon_r)$ is about 2.409.

Conclusions

The major conclusions that are drawn from the present experimental investigations are listed below:

- There is a definite limit curve for the onset of wrinkling which can be represented in terms of the strain increments ratio and the stress ratio.
- The Aluminium 5086 alloy annealed at temperature 300 °C is superior in suppressing the wrinkles comparing with the sheets, annealed at other two temperatures.
- The wrinkling limit value (β) according to the theory and the experiment matches each other.
- Material having high n value, high *R*-value and high UTS/σ_y ratio suppresses the wrinkling.

- Wrinkling limit diagrams drawn in terms of strain increments ratio is highly suitable for the study of wrinkling behaviour of sheet metals
- Using Finite Element Method and crystal plasticity theory the wrinkling theory can be further strengthened for different types of metals.

References

1. Rangaraju N, Raghuram T, Vamsi Krishna B, Prasad Rao K, Venugopal P (2005) Mater Sci Eng A 398:246
2. Takuda H, Yamazaki N, Hatta N, Kikuchi S (1995) J Mater Sci 30:957
3. Ravi Kumar D, Swaminathan K (1999) Mater Sci Technol 15:1241
4. Tvergaard V (1981) Int J Frac 17:389
5. Gunasekara JS, Thompson PF (1982) In: Manufacturing engineering transactions, 10th NAMRC, pp 173–179
6. Keelar SP, Stine PA (1989) SAE Tech Pap Ser 890345:25
7. Mazilu P (1987) In: Predeleanu M (ed) Computational methods for predicting material processing defects. Elsevier, Amsterdam, pp 263–274
8. Narayanasamy R, Sowerby R (1993) J Mater Proc Tech 39:43
9. Sowerby R, Karima M, Chakravarti PC (1982) J Mech Work Tech 6:35
10. Szacinzki AM, Thomson PF (1991) J Mater Proc Tech 25:125
11. Szacinzki AM, Thomson PF (1991) J Mater Proc Tech 7:224
12. Loganathan C, Narayanasamy R (2005) J Mat Sci Eng 406:229
13. Wang XF, Lee LHN (1989) J Eng Mater Tech 111:235
14. Narayanasamy R, Sowerby R (1994) J Mater Proc Tech 41:275
15. Karima M, Sowerby R (1980) Report No.144. Faculty of Engineering, McMaster University, Hamilton, Ontario, Canada
16. Narayanasamy R, Sowerby R (1994) J Mater Proc Tech 41:275
17. Di S, Thomson PF (1997) J Testing Eval JTEVA 25(1):74
18. Wang J, Wu X, Thomson PF, Flitman A (2000) J Mater Proc Tech 105:215
19. Kim Y, Son Y (2000) J Mater Proc Tech 97:88
20. Hill R (1950) Mathematical theory of plasticity, Ch. 12. Oxford Univ. Press, London
21. Hutchinson JW (1974) In: Yin CS (ed) Advances in applied mechanics, vol 14, pp 215–220
22. Narayanasamy R (1992) Drawability of sheet metals through conical and tractrix dies. Ph.D. thesis, Regional Engineering College, Tiruchirappalli, India
23. Karima M (1981) Ph.D. thesis, McMaster University, Hamilton, Ontario, Canada
24. Wang CT, Kinzel G, Altan T (1994) Int J Mater Proc Tech Sci 36(10):945
25. Court SA, Gatenby KM, Lloyd DJ (2001) Mater Sci Eng A 319/21:443
26. Davis R (ed) (1993) Aluminium and aluminium alloys, ASM international, Material Park, OH
27. Narayanasamy R, Sathiya Narayanan C (2005) Indian J Eng Mater Sci 12:141
28. Narayanasamy R, Loganathan C (2006) Mater Sci Eng A 419(1–2):249